AAS 19-505

FRACTIONAL CONTROL IN LINEARIZED RELATIVE-ORBIT DYNAMICS

David Yaylali[*], Eric Butcher[†], and Andrew J. Sinclair[‡]

Fractional control strategies for linearized relative-orbit dynamics are introduced and compared to standard proportional-derivative control strategies. Using fractional derivative operators in the controller introduces additional tunable degrees of freedom, affording more freedom in shaping the controlled trajectory. As a result, more optimal rendezvous trajectories can be achieved. Specifically, it is shown that fractional relative-orbit controllers outperform standard controllers in terms of several important performance measures such as settling time, overshoot, and control effort.

INTRODUCTION

Continuous control strategies for the relative motion of two or more spacecraft (SC), each in its own orbit about a celestial body, are important in many practical applications including SC formation flying, approach, and rendezvous. When the SC of interest are in close proximity, the nonlinear second-order equations of motion describing the relative motion can be linearized (see, *e.g.*, References 1 and 2). In these cases it is straightforward to construct linear control laws which utilize the relative distance and velocity between the SC for the purpose of feedback control. Since position and velocity data are used, these control laws essentially consist of proportional-derivative (PD) or proportional-integral-derivative (PID) controllers, and the controlled trajectories can be shaped by adjusting the set of proportional, integral, and derivative gains.

The ability to shape the controlled trajectory is perhaps the main reason why PD and PID controllers are so widely used in industrial and GNC applications. By adjusting the N controller gains independently, one can (in best-case scenarios) adjust N separate performance measures characterizing the trajectory of the controlled system. In many cases, however, certain performance measures can be coupled (*i.e.*, settling time and overshoot in PD-controlled second-order systems) so that the amount of freedom one has in separately adjusting these performance measures is reduced. It may therefore be desirable to introduce additional tunable parameters into the controller in order to more freely adjust the controller performance or controlled trajectory. One innovative way of introducing such extra degrees of freedom in proportional-derivative controllers is by adjusting the action of the derivatives themselves.

Fractional calculus offers ways to assign meaning to non-integer orders of the differentiation and

[*]MS Student, Department of Aerospace and Mechanical Engineering, University of Arizona, Tucson, AZ 85721
[†]Professor, Department of Aerospace and Mechanical Engineering, University of Arizona, Tucson, AZ 85721
[‡]Senior Aerospace Engineer, Space Vehicles Directorate, Air Force Research Laboratory, Kirtland AFB, NM 87117

integration operators.[3–5] In other words, fractional calculus explores the generalization

$$\left(\frac{d}{dx}\right)^{\text{integer}} \longrightarrow \left(\frac{d}{dx}\right)^{\text{real or complex}}$$

Although presently a rather obscure subject, a vision of fractional calculus was in fact evident to the pioneers of the ordinary, integer-order calculus including Leibniz, and some years later Euler. It was not until the latter half of the 20th century, however, when applications of these formal concepts began to appear. Natural and mechanical systems which are more accurately or efficiently modeled by fractional-order differential equations of motion include lossy transmission lines, heat diffusion into semi-infinite solids, damping of a plate suspended in viscous liquid, fluid flow and rheology, and certain electric circuits (see References 6 and 7 for reviews). Bagley and Calico[8] found that viscoelastically damped structures exhibit behavior which is more efficiently described by fractional differential equations, developed a fractional state-space formalism which simplified the description of such systems, and suggested the use of fractional feedback control.

Fractional control strategies were developed in the late 20th century, led in large part by investigations by Oustaloup[9] and Podlubney.[10] In some cases, one seeks to control a system whose equations of motion involve non-integer-order derivatives or integrals; in others, one may seek to design controllers for integer-order systems using fractional derivatives or integrals of the system's state. In both cases, the closed-loop equations of motion for the system become fractional in nature. Investigations by Matignon,[11] among others, led to important contributions in the understanding of stability of such systems. One of Podlubney's larger contributions was, as alluded to above, the generalization of PID controllers to fractional order $\text{PI}^{\mu}\text{D}^{\nu}$ controllers,[10] with integral and derivative control of order μ and ν, respectively, where $0 < \mu, \nu \leq 1$; integer-order PID control is obtained with $\mu = \nu = 1$. The fractional orders therefore act as additional "knobs" one can tune in order to shape the trajectory of the controlled closed-loop system. Moreover, in certain cases and in terms of specific performance measures, these fractional $\text{PI}^{\mu}\text{D}^{\nu}$ controllers have been shown to outperform their integer-order counterparts (see, *e.g.*, References 12 and 13).

Fractional $\text{PI}^{\mu}\text{D}^{\nu}$ control has been used for spacecraft attitude control, where certain performance criteria such as settling time and overshoot were simultaneously optimized.[14–16] The application and refinement of integer-order PD control for linearized relative orbit dynamics has been thoroughly explored.[17–19] To the best of our knowledge, however, fractional control for linearized relative orbit dynamics has not been previously explored.

In this work we will introduce fractional PD^{α}-type relative-orbit controllers. We will first briefly review relative-orbit dynamics and control, and introduce the necessary fractional calculus needed to construct fractional controllers. A fractional PD^{α}-type fractional controller for linearized relative-orbit motion will then be introduced, and stability conditions and strategies for controller design will be discussed. The performance and resulting trajectories of these controllers will then be explored numerically for three benchmark relative-orbit configurations, demonstrating that fractional controllers can outperform standard controllers for relative-orbit maneuvering. We will then conclude by summarizing our results and highlighting directions for future research.

BACKGROUND FORMALISM

The term "relative orbit" entails describing the relative motion of two (or more) spacecraft in orbit about a common celestial body. In relative-orbit dynamics it is typical to elevate the status of one

spacecraft and refer to this as the *chief*, and refer to the second SC as the *deputy*. At any given time each spacecraft will be described by its own set of orbit elements, $\boldsymbol{\epsilon}$ and $\boldsymbol{\epsilon}_d$ (where un-subscripted variables will always be associated with the chief). The orbit element difference is $\delta\boldsymbol{\epsilon} = \boldsymbol{\epsilon}_d - \boldsymbol{\epsilon}$, and the full state of the two-SC system can then be parameterized by the 12-element set $\{\boldsymbol{\epsilon}, \delta\boldsymbol{\epsilon}\}$.

To characterize the relative-orbit trajectory of the deputy it is convenient to attach a reference frame to chief. A standard choice is the *local-vertical, local-horizontal* (LVLH) frame, also known as the *Hill* frame, which is defined by the orthonormal triplet of basis vectors

$$\hat{\boldsymbol{x}} = \frac{\boldsymbol{r}}{r}; \quad \hat{\boldsymbol{y}} = \hat{\boldsymbol{z}} \times \hat{\boldsymbol{x}}; \quad \hat{\boldsymbol{z}} = \frac{\boldsymbol{h}}{h}. \tag{1}$$

Here $\boldsymbol{r}$ (with $r = |\boldsymbol{r}|$) is the Earth-centered inertial (ECI) position vector of the chief and $\boldsymbol{h}$ (with $h = |\boldsymbol{h}|$) is the angular momentum vector of the chief orbit. The motion in the $\hat{\boldsymbol{z}}$ direction is therefore referred to as *out-of-plane* motion, and motion in the $\hat{\boldsymbol{x}}$ and $\hat{\boldsymbol{y}}$ plane is referred to as *in-plane motion*. Since the chief orbits about the ECI reference frame, the LVLH frame is non-inertial.

The individual dynamics of the chief and deputy are described by Newton's law of universal gravitation, and the solutions for bound trajectories are described by Keplerian ellipses and the motion is periodic. In contrast, the relative-orbit trajectory of the deputy from the reference frame of the chief is in general non-periodic; in the LVLH-frame of the chief, the dynamics of the deputy are given by

$$\ddot{x} = 2\dot{f}\left(\dot{y} + y\frac{\dot{r}}{r}\right) + x\dot{f}^2 + \frac{\mu}{r^2} - \frac{\mu}{r_d^3}(r + x) \tag{2a}$$

$$\ddot{y} = -2\dot{f}\left(\dot{x} + x\frac{\dot{r}}{r}\right) + y\dot{f}^2 - \frac{\mu}{r_d^3}y \tag{2b}$$

$$\ddot{z} = -\frac{\mu}{r_d^3}z, \tag{2c}$$

where f is the instantaneous true anomaly of the chief, r_d is the magnitude of the ECI position vector of the deputy, and μ is the gravitational parameter of the central gravitating body. In general, the chief orbital radius r is time-dependent. Since this is a second-order system in three dimensions, the full state of the deputy can be characterized at any time by the 6-element vector $\boldsymbol{x} = [x, y, z, \dot{x}, \dot{y}, \dot{z}]^T$ comprising the LVLH deputy position and velocity. Furthermore, since the LVLH frame itself is defined by the 6-element set of chief orbital elements $\boldsymbol{\epsilon}$, the full state of the relative orbit trajectory can again be characterized by a 12-element set of quantities, $\{\boldsymbol{\epsilon}, \boldsymbol{x}\}$. Transformations between the orbital element description $\{\boldsymbol{\epsilon}, \delta\boldsymbol{\epsilon}\}$ and the LVLH description $\{\boldsymbol{\epsilon}, \boldsymbol{x}\}$ are nonlinear and are straightforward to derive.

In this work we will be concerned with close-proximity maneuvers, so that the LVLH components $\{x, y, z\}$ are small compared to the instantaneous radius of the chief orbit. Furthermore, for simplicity we will assume that the chief orbit is approximately circular, so that chief orbital radius $r = a$ is no longer time-dependent; relaxation of these simplifying assumptions will be discussed in the Conclusions. In this case, Eqs. (2) reduce to the *Hill-Clohessey-Wiltshire* (HCW) equations[17]

$$\ddot{x} = 2n\dot{y} + 3n^2x \tag{3a}$$

$$\ddot{y} = -2n\dot{x} \tag{3b}$$

$$\ddot{z} = -n^2z, \tag{3c}$$

where the constant $n = \sqrt{\mu/r^3}$ is the mean motion of the (circular) chief orbit. Moreover, in these close-proximity cases, the transformation from the inertial frame state $\{\boldsymbol{\epsilon}, \delta\boldsymbol{\epsilon}\}$ and the LVLH state $\{\boldsymbol{\epsilon}, \boldsymbol{x}\}$ can be linearized as $\boldsymbol{x} = \Lambda(\boldsymbol{\epsilon})\delta\boldsymbol{\epsilon}$, where the transformation matrix Λ was given in, *e.g.*, Reference 18. The relationship between the nonlinear and linearized equations of motion, along with the nonlinear and linearized state transformations, can be utilized to more accurately propagate the linearized solution through a process known as linearization calibration.[18]

Relative-Orbit Control Systems for HCW Dynamics

A common control strategy for relative-orbit maneuvering is to apply to the deputy some control thrust (while the chief follows its uncontrolled natural trajectory). This strategy is convenient in many practical scenarios, such as in cases where a small deputy spacecraft attempts to rendezvous with a space station or a chief with much larger mass. To capture the dynamics of this control strategy, control accelerations are added to the right-hand sides, for each component, in either Eqs. (2) or Eqs. (3). In the case of controlled linearized dynamics, calibration can again be utilized[19] to mitigate propagation inaccuracies injected through linearization error.

To avoid large numerical differences in controller design parameters in what follows, we choose to work with the dimensionless HCW equations, found by scaling the physical variables as

$$(\text{length}) \to (\text{length})/r, \qquad (\text{time}) \to (\text{time})/T_{\text{orb}},$$

with chief orbital radius r and chief orbital period $T_{\text{orb}} = 2\pi/n$. That is, we change variables as

$$x \to u = \frac{x}{r}, \quad y \to v = \frac{y}{r}, \quad z \to w = \frac{z}{r}, \quad t \to s = nt. \tag{4}$$

The time coordinate is therefore transformed to an angular coordinate corresponding to the chief's true anomaly. The dimensionless form of the HCW equations, under control input $\boldsymbol{\upsilon} = [\upsilon_u, \upsilon_v, \upsilon_w]^T$, is now given by

$$\begin{aligned} u'' &= 2v' + 3u + \upsilon_u \\ v'' &= -2u' + \upsilon_v \\ w'' &= -w + \upsilon_w \end{aligned}$$

where $(\cdot)'$ represents a derivative with respect to s. Defining the dimensionless state $\boldsymbol{\chi} = [\boldsymbol{\xi}^T \; \boldsymbol{\xi}'^T]^T$, with $\boldsymbol{\xi} = [u \;\; v \;\; w]^T$, these dynamics can be recast into the form of a first-order state equation

$$\boldsymbol{\chi}' = \begin{bmatrix} \mathbf{0} & I_3 \\ A_1 & A_2 \end{bmatrix} \boldsymbol{\chi} + \begin{bmatrix} \mathbf{0} \\ I_3 \end{bmatrix} \boldsymbol{\upsilon}, \quad A_1 = \begin{bmatrix} 3 & 0 & 0 \\ 0 & 0 & 0 \\ 0 & 0 & -1 \end{bmatrix}, \; A_2 = \begin{bmatrix} 0 & 2 & 0 \\ -2 & 0 & 0 \\ 0 & 0 & 0 \end{bmatrix}. \tag{5}$$

All physical trajectories and results can be found by rescaling back to physical units through Eqs. (4); *e.g.*, the dimensionless control input $\boldsymbol{\upsilon}$ corresponds to physical control acceleration $\boldsymbol{u} = rn^2\boldsymbol{\upsilon}$.

If the deputy spacecraft is capable of measuring both its relative position and velocity with respect to the chief, these data can be used in a full-state feedback controller of the form

$$\boldsymbol{\upsilon} = -K\boldsymbol{\chi} = -\begin{bmatrix} K_P & K_D \end{bmatrix} \begin{bmatrix} \boldsymbol{\xi} \\ \boldsymbol{\xi}' \end{bmatrix},$$

allowing us to write the closed-loop equations of motion as

$$\boldsymbol{\chi}' = \begin{bmatrix} \mathbf{0} & I_3 \\ A_1 - K_P & A_2 - K_D \end{bmatrix} \boldsymbol{\chi}. \tag{6}$$

As suggested by the choice of notation, this controller takes the form of a PD controller. The proportional and derivative gain matrices K_P and K_D are of dimension 3×3 and in general contain nonzero off-diagonal elements.

Due to the off-diagonal elements in A_2, the natural HCW dynamics give rise to a coupling between the u and v components. Since the natural w-component dynamics decouple, there is no conceivable reason why one would introduce uw- or vw-coupling through controller gains. It is therefore reasonable to set these coupling gains to zero, so that

$$K_P = \begin{bmatrix} k_{P_u} & k_{P_{uv}} & 0 \\ k_{P_{vu}} & k_{P_v} & 0 \\ 0 & 0 & k_{P_w} \end{bmatrix} = \begin{bmatrix} \mathcal{K}_P & \mathbf{0}_{2\times1} \\ \mathbf{0}_{1\times2} & k_{P_w} \end{bmatrix}, \quad K_D = \begin{bmatrix} k_{D_u} & k_{D_{uv}} & 0 \\ k_{D_{vu}} & k_{D_v} & 0 \\ 0 & 0 & k_{D_w} \end{bmatrix} = \begin{bmatrix} \mathcal{K}_D & \mathbf{0}_{2\times1} \\ \mathbf{0}_{1\times2} & k_{D_w} \end{bmatrix}, \tag{7}$$

which in turn allows us to separate the HCW dynamics Eq. (5) into two separate subsystems describing, respectively, the in-plane and out-of-plane dynamics.

The in-plane (u- and v-component) closed-loop dynamics are given by

$$\boldsymbol{\zeta}' = \left(\begin{bmatrix} \mathbf{0} & I_2 \\ \bar{A}_1 & \bar{A}_2 \end{bmatrix} - \begin{bmatrix} \mathbf{0} & I_2 \\ \mathcal{K}_P & \mathcal{K}_D \end{bmatrix} \right) \boldsymbol{\zeta} = \begin{bmatrix} \mathbf{0} & I_2 \\ \Sigma_1 & \Sigma_2 \end{bmatrix} \boldsymbol{\zeta}, \tag{8}$$

with $\boldsymbol{\zeta} = [\boldsymbol{\sigma}^T \;\; \boldsymbol{\sigma}'^T]^T$, $\boldsymbol{\sigma} = [u \;\; v]^T$, and where $\bar{A}_1$ and $\bar{A}_2$ are the top-left 2×2 submatrices of A_1 and A_2, respectively. The closed-loop matrices $\Sigma_1 = \bar{A}_1 - \mathcal{K}_P$ and $\Sigma_2 = \bar{A}_2 - \mathcal{K}_D$ are explicitly given by

$$\Sigma_1 = \begin{bmatrix} 3 - k_{P_u} & -k_{P_{uv}} \\ -k_{P_{vu}} & -k_{P_u} \end{bmatrix}, \; \Sigma_2 = \begin{bmatrix} -k_{D_u} & 2 - k_{D_{uv}} \\ -2 - k_{D_{vu}} & -k_{D_v} \end{bmatrix}. \tag{9}$$

In general, Eq. (8) describes a coupled two-dimensional damped harmonic oscillator.

The decoupled out-of-plane (w-component) dynamics are given by

$$\begin{bmatrix} w' \\ w'' \end{bmatrix} = \begin{bmatrix} 0 & 1 \\ -(1 + k_{P_w}) & -k_{D_w} \end{bmatrix} \begin{bmatrix} w \\ w' \end{bmatrix}, \tag{10}$$

which is equivalent to the state equation describing a single damped harmonic oscillator with spring and damping coefficients $1 + k_{P_w}$ and k_{D_w}, respectively.

For both in-plane (Eq. (8)) and out-of-plane (Eq. (10)) dynamics, the control system comprises two types of tunable parameters: the proportional-type gains feeding back LVLH position differences, and the derivative-type gains feeding back LVLH velocity differences. As introduced above, these PD-controlled systems can be thought of as a damped harmonic oscillators, with P-type gains corresponding to spring-stiffness constants and D-type gains corresponding to damping coefficients. This analogy tells us how each gain affects the trajectory of the controlled system. For instance, increasing the P-type gains has the effect of "speeding up" the response of the system while increasing the amount of "overshoot". On the other hand, increasing the D-type gains has the opposite effect of slowing down the response of the system while reducing overshoot. It is therefore intuitively apparent that, by adjustment of these gains, one has limited ability to shape the controlled trajectory of the system. This limited freedom in shaping the system trajectory serves as motivation for introducing a new, unique, tunable parameter in the relative-orbit controller.

Fractional Calculus and Control

We will achieve a generalization of HCW PD-type controllers introduced above,

$$\boldsymbol{\upsilon} = -K_P\boldsymbol{\xi} - K_D D^1\boldsymbol{\xi}, \tag{11}$$

through a generalization of the derivative operator D^1. This latter generalization can be conceptually expressed as

$$\begin{aligned} \frac{d^n f(t)}{dt^n} \equiv D^n f(t), \quad n \in \mathbb{N} \quad &\longrightarrow \quad D^\alpha f(t), \quad \alpha \in \mathbb{R}^+ \\ \int\cdots\int f(t) \underbrace{dt\cdots dt}_{n \text{ times}} \equiv D^{-n} f(t), \quad n \in \mathbb{N} \quad &\longrightarrow \quad D^{-\nu} f(t), \quad \nu \in \mathbb{R}^+. \end{aligned}$$

These generalizations assign meaning to "non-whole" derivatives and integrals (*e.g.*, $\frac{d^{0.5}f(x)}{dx^{0.5}} = D^{0.5}f(x)$). There are in fact a number of different definitions for the fractional D^α operators;[4] we will exclusively use the Caputo fractional derivative,[20] which is defined in terms of the Riemann-Liouville fractional integral. The Riemann-Liouville (RL) fractional integration operator of order ν is given by

$${}_aD_t^{-\nu} f(t) \equiv \frac{1}{\Gamma(\nu)} \int_a^t (t-\tau)^{\nu-1} f(\tau) d\tau, \quad t > a, \;\; \nu > 0, \tag{12}$$

where Γ is Euler's *gamma function*, which generalizes the factorial to real and complex numbers. The RL integral is well defined if f is piecewise continuous on (a, ∞) and integrable on any finite subinterval of $[a, \infty)$. That is, ${}_aD_t^{-\nu} f(t)$ is defined for *locally integrable* functions, $f \in L^1_{\text{loc}}[a, t)$. Note that power functions $t^p, \; p > -1$, satisfy these conditions. The Caputo derivative operator of order α is then given by

$${}_aD_t^{\alpha} f(t) \equiv {}_aD_t^{-(n-\alpha)} \left[\frac{d^n f(t)}{dt^n} \right], \quad t > a, \;\; \alpha > 0, \;\; n = \lceil \alpha \rceil, \tag{13}$$

where $\lceil \cdot \rceil$ represents the ceiling function. Since this is an RL integral of an integer-order derivative of f, we require that f is differentiable to order n, and that $f^{(n)}(t) \in L^1_{\text{loc}}[a, t)$.

In this work, we will exclusively take the lower terminal of the integral to be zero; we therefore will suppress the lower indices when this is the case,

$${}_0D_t^{\alpha} \to D^\alpha.$$

Despite this notational simplification, one should remain mindful that, unlike ordinary derivatives, fractional derivatives are *non-local* and depend on the history of the functions on which they act. It should also be mentioned that, since we are considering second-order dynamics (*i.e.*, the spacecraft have *inertia*), it will be understood that all trajectories under consideration are continuous and differentiable, and thus satisfy the modest continuity and differentiability requirements necessary for the validity of the Caputo derivative. In particular, trajectories can be expanded as power series, with the Caputo derivative of a power function explicitly given by

$$D^\alpha t^p = \frac{\Gamma(p+1)}{\Gamma(p-\alpha+1)} t^{p-\alpha}, \quad \alpha \in \mathbb{R}^+, \; p > 0, \tag{14}$$

and in this case the standard *law of exponents* for derivatives holds: $D^{\alpha}D^{\beta}t^{p} = D^{\alpha+\beta}t^{p}$, $\alpha, \beta \in \mathbb{R}^{+}$.

As alluded to above, we will generalize the relative orbit PD controller discussed above by introducing fractional derivatives in the control law. The closed-loop equations of motion will then take the form of fractional differential equations (FDEs). Although FDEs can in some cases be solved analytically, we will utilize numerical methods to simulate relative-orbit trajectories under fractional control. Specifically, to propagate FDEs numerically we will utilize the fractional Chebyshev collocation (FCC) method.[21,22] This method approximates a solution as an N^{th} order expansion in Chebyshev polynomials, so that fractional derivatives of this solution can be evaluated via Eq. (14). To compute the trajectory using FCC, the N coefficients of the polynomial are solved by evaluating the FDE at N collocation points (time points) within the integration window, which we take to be the Chebyshev-Gauss-Lobatto points (the extrema of the Chebyshev polynomials). These collocation points are more densely distributed near the endpoints of the integration window, thus mitigating the so-called *Runge's phenomenon*.

FRACTIONAL CONTROL FOR HCW DYNAMICS

The fractional derivative can now be used in place of the integer-order derivative in Eq. (11), forming the *fractional* PD$^{\alpha}$ HCW controller

$$\boldsymbol{\upsilon} = -K_P\boldsymbol{\xi} - K_D D^{\boldsymbol{\alpha}}\boldsymbol{\xi}, \tag{15}$$

where $D^{\boldsymbol{\alpha}}\boldsymbol{\xi} \equiv [D^{\alpha_u}u \;\; D^{\alpha_v}v \;\; D^{\alpha_w}w]^T$ and $\{\alpha_u, \alpha_v, \alpha_w\} \in [0, 1]$. That is, our controller feeds back LVLH positions and *fractional derivatives* of the positions, with fractional derivative orders for each component now separately tunable. The closed-loop equations of motion become

$$\boldsymbol{\chi}' = \begin{bmatrix} \mathbf{0} & I_3 \\ A_1 - K_P & A_2 \end{bmatrix}\boldsymbol{\chi} - \begin{bmatrix} \mathbf{0} \\ K_D \end{bmatrix}\begin{bmatrix} D^{\alpha_u}u \\ D^{\alpha_v}v \\ D^{\alpha_w}w \end{bmatrix}. \tag{16}$$

Due to the presence of the fractional derivatives, we are no longer able to write this controller in full-state feedback form $\boldsymbol{\upsilon} = -K\boldsymbol{\chi}$, which in turn prevents us from writing the closed-loop equations of motion as in Eq. (6). Using the gain matrices given in Eq. (7), however, the closed-loop equations of motion again decouple into in-plane and out-of-plane dynamics as

$$\boldsymbol{\zeta}' = \begin{bmatrix} \mathbf{0} & I_2 \\ \bar{A}_1 - \mathcal{K}_P & \bar{A}_2 \end{bmatrix}\boldsymbol{\zeta} - \begin{bmatrix} \mathbf{0} \\ \mathcal{K}_D \end{bmatrix}\begin{bmatrix} D^{\alpha_u}u \\ D^{\alpha_v}v \end{bmatrix}. \tag{17}$$

and

$$\begin{bmatrix} w' \\ w'' \end{bmatrix} = \begin{bmatrix} 0 & 1 \\ -(1 + k_{P_w}) & 0 \end{bmatrix}\begin{bmatrix} w \\ w' \end{bmatrix} - \begin{bmatrix} 0 \\ k_{D_w} \end{bmatrix} D^{\alpha_w}w, \tag{18}$$

respectively (*c.f.*, Eqs. (8) and (10)). The latter equation describes a *fractionally damped* harmonic oscillator in 1 dimension, which in second-order form is written as

$$w'' + k_{D_w}D^{\alpha_w}w + (1 + k_{P_w})w = 0, \tag{19}$$

while the former equation again describes a 2-dimensional coupled system.

Stability

For LTI systems such as Eq. (6), which we can write in shorthand as $\boldsymbol{\chi}' = A_{CL}\boldsymbol{\chi}$, the stability of the equilibrium point $\boldsymbol{\chi}^* = [\boldsymbol{\xi}^{*T}\ \boldsymbol{\xi}'^{*T}]^T = \mathbf{0}$ is guaranteed if the eigenvalues of the closed-loop system matrix A_{CL} lie in the left-half complex plane (or, equivalently, if A_{CL} is *Hurwitz*). That is, for any given initial condition $\boldsymbol{\chi}(0) = \boldsymbol{\chi}_0$, the trajectory approaches the equilibrium point (*i.e.*, the chief-deputy system achieves rendezvous) asymptotically, $\boldsymbol{\chi}(s) \to 0$ as $s \to \infty$. This follows from the fact that the state-transition matrix (STM) describing the state evolution, $\boldsymbol{\chi}(s) = \Phi(s,0)\boldsymbol{\chi}_0$, can be evaluated as

$$\Phi(s,0) = e^{A_{CL}s},$$

and through modal decomposition it can be seen that $\Phi(s,0)$ vanishes asymptotically if and only if the real part of all eigenvalues of A_{CL} are negative.

In the case of fractionally controlled relative-orbit dynamics, Eq. (17), we are no longer able to write the closed-loop equations of motion as $\boldsymbol{\chi}' = A_{CL}\boldsymbol{\chi}$, and therefore the above stability condition does not apply. For fractional systems where the fractional orders are rational, $\{\alpha_u, \alpha_v, \alpha_w\} \in \mathbb{Q}$, however, it is possible to express the closed-loop dynamics as a *pseudostate* equation

$$D^{\alpha}\tilde{\boldsymbol{\chi}} = \tilde{A}_{CL}\tilde{\boldsymbol{\chi}}. \tag{20}$$

Here $\tilde{\boldsymbol{\chi}}$ is the *pseudostate* corresponding to the system and α is the *commensurate* fractional order of the system, such that all derivatives orders of the system, $\{1, 2, \alpha_u, \alpha_v, \alpha_w\}$, are integer multiples of α. The pseudostate is a higher-dimensional representation of the state $\boldsymbol{\chi}$, given explicitly by $\tilde{\boldsymbol{\chi}} = [\boldsymbol{\xi}^T, D^{\alpha}\boldsymbol{\xi}^T, D^{2\alpha}\boldsymbol{\xi}^T,\ \ldots, D^{(m-1)\alpha}\boldsymbol{\xi}^T]^T$, and thus the pseudostate system matrix $\tilde{A}_{CL}$ is of dimension $(3m \times 3m)$. Analogous to the case of integer-order LTI systems, the *pseudostate transition matrix* (pSTM) can be expressed as

$$\tilde{\Phi}(s,0) = E_{\alpha}(A_{CL}s^{\alpha}), \tag{21}$$

where E_{α} is the *Mittag-Leffler function* which can be thought of as a generalization of the exponential function (such that $E_{\alpha}(z) \to \exp(z)$ as $\alpha \to 1$). By considering the modal decomposition of $\tilde{\Phi}$, it can be shown that $\tilde{\boldsymbol{\chi}}$ asymptotically vanishes, and thus the fractionally controlled relative-orbit system is asymptotically stable, if and only if the $3m$ eigenvalues λ_i of $\tilde{A}_{CL}$ satisfy

$$|\arg\lambda_i| > \alpha\frac{\pi}{2}, \quad i = 1, 2, \ldots, 3m. \tag{22}$$

This condition is an instance of *Matignon's theorem*,[11] and reduces to the standard left-half-plane eigenvalue condition for integer-order systems when $\alpha \to 1$ (See Fig. 1). For a more detailed exposition of stability for fractionally-controlled systems, we refer the reader to Reference 23.

It should be noted that, although the eigenvalues of $\tilde{A}_{CL}$ (and thus the stability of the fractionally-controlled system) depend on the gain choices within K_P and K_D, we will not in this work utilize this condition in controller design. This condition, however, is indeed satisfied for all optimized controllers considered in the following sections. We also note that the above discussion applies to the *linearized* HCW dynamics, with linearization error increasing with the relative chief-deputy distance. The above eigenvalue conditions thus only guarantee *local* asymptotic stability.

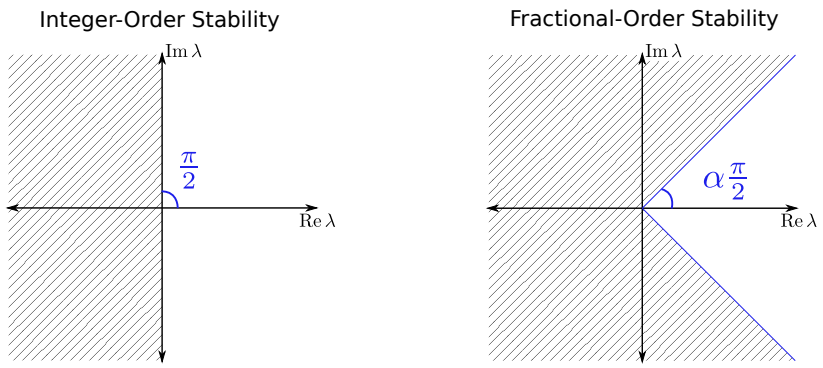

Figure 1. An illustration of Matignon's stability theorem for fractional order systems, *e.g.*, Eq. (20). Eigenvalues of the (pseudo)state-equation system matrix must be within the shaded regions for system stability.

Controller Design

The fractional relative-orbit controller introduced above has 13 tunable parameters: 10 proportional and derivative gains in $\mathcal{K}_P$, $\mathcal{K}_D$, k_{P_w}, and k_{D_w}, along with the three tunable fractional orders α_u, α_v, and α_w. Since the in-plane and out-of-plane motion decouples, this control design problem is slightly simplified: one must design an in-plane controller with 10 free parameters, and a separate out-of-plane controller with three free parameters. Nevertheless, with this large amount of freedom, and moreover due to the fact that much of the controller parameter space leads to unstable trajectories, some controller *design strategy* is needed.

For standard controllers where $\{\alpha_u, \alpha_v, \alpha_w, \} \to 1$, various design strategies can be used. One such strategy is to decouple *all* components through a proper choice of off-diagonal gains. This can be achieved by choosing $k_{P_{vu}} = k_{P_{uv}} = 0$ and $k_{D_{uv}} = -k_{D_{vu}} = 2$ in Eq. (9), giving rise to three dynamical equations, each corresponding to a 1D damped harmonic oscillator. One can then choose the damping and spring-constant coefficients in order to achieve some desired trajectory; for instance, in each component the gains can be tuned such that the motion in each component is critically damped.

A second design strategy in the case of integer-order control is to treat the closed-loop system in Eq. (5) as an optimal control problem, and derive the controller by defining some cost functional $J\{\boldsymbol{\chi}(\boldsymbol{\upsilon})\}$. By varying J with respect to control $\boldsymbol{\upsilon}$ we can find the extremum of J, which in turn provides the optimal $\boldsymbol{\upsilon}$ through the standard machinery of optimal control theory. For instance, by defining a cost function to be quadratic in the trajectory $\boldsymbol{\chi}$ and control $\boldsymbol{\upsilon}$,

$$J = \int_0^\infty \left(\boldsymbol{\chi}^T Q \boldsymbol{\chi} + \boldsymbol{\upsilon}^T R \boldsymbol{\upsilon}\right) ds, \tag{23}$$

this becomes the familiar *linear quadratic regulator* (LQR) problem; the controller which minimizes this cost is $\boldsymbol{\upsilon} = -R^{-1}B^T P \boldsymbol{\chi}$, where P is the solution to the associated (continuous-time) algebraic Riccati equation.

For the fractional controller, however, these design strategies run into complications. In the first strategy, due to the presence of fractional derivative control terms, Eq. (16) can no longer be decoupled into separate u and v dynamics by proper choice of gains. In other words, within Eq. (16), since $\bar{A}_2$ are the coefficients of $[D^1 u \; D^1 v]^T$ and $\mathcal{K}_D$ are the coefficients of $[D^{\alpha_u} u \; D^{\alpha_v} v]^T$, there

is no choice of gains within $\mathcal{K}_D$ which can cancel the off-diagonal terms in $\bar{A}_2$.* In the second strategy, since our dynamical equations are now fractional in nature, an analogous formalism of optimal *fractional* control needs to be utilized. Although the variational fractional calculus has been explored in the literature,[24,25] application of these concepts to all but the simplest of dynamical systems is far from straightforward.

A third design strategy, however, faces no similar complications, and is well-suited for our present purposes: given some performance measure ψ, a *numerical survey* over the controller parameter space can be performed to find the specific controller which optimizes ψ. Although this is a computational intensive strategy, it will serve to concretely demonstrate that fractional controllers can outperform integer-order controllers. Moreover, fractional and integer-order controllers in this scheme are treated on equal footing, as the integer-order controllers simply correspond to the edges of the $\{\alpha_u, \alpha_v\}$ parameter-space survey window. More elegant and/or practical design strategies will be left as topics for future work.

NUMERICAL SURVEY OF PARAMETER SPACE

In order to demonstrate that the fractional relative-orbit controller can outperform the standard integer-order controller, a number of example trajectories, along with various performance measures characterizing these trajectories, will be computed. In almost all cases considered herein, the performance measure under consideration becomes optimal when the fractional orders of the derivatives are tuned away from unity. These examples thus serve as a *proof-of-principle*, illustrating that the fractional PD$^\alpha$ controller can in many cases outperform the standard PD controller.

To this end, we will consider three benchmark initial conditions $\boldsymbol{\chi}_0$, corresponding to three different relative position/velocity configurations of the deputy with respect to the chief. These initial conditions (in terms of LVLH coordinates) are listed in Table 1, and in all cases the chief orbit defining the LVLH is given by the orbital elements

$$\boldsymbol{\epsilon}_0 = [a,\ q_1,\ q_1,\ i,\ \Omega,\ \theta] = [10^4\ \text{km},\ 0^\circ,\ 20^\circ,\ 0,\ 0,\ 0^\circ].$$

Since the classical orbital elements ω (argument of periapsis) and f (true anomaly) are undefined for circular orbits, we have here chosen to use the alternative orbital elements $\theta = \omega + f$ (argument of latitude), $q_1 = e\sin\omega$, and $q_2 = e\cos\omega$. In terms of these initial chief OEs, the initial conditions in Table 1 correspond to approximately the following orbit element differences:

$$\begin{aligned}
&\text{IC1:}\quad \delta q_1 \approx 0.001,\ \delta i \approx 0.1^\circ,\\
&\text{IC2:}\quad \delta q_1 \approx 0.001,\ \delta\Omega \approx 0.17^\circ,\ \delta\theta \approx -0.05^\circ\\
&\text{IC3:}\quad \delta a \approx 80\ \text{km},\ \delta q_1 \approx 0.007,\ \delta i \approx -0.1^\circ,\ \delta\Omega \approx -0.17^\circ,\ \delta\theta \approx 0.05^\circ.
\end{aligned}$$

To quantify and compare the performance of different controllers, we define the settling time, overshoot, and integrated control effort for relative orbit trajectories as follows:

- **Settling Time (ST):** the dimensionless quantities $s_i = n\tau_i$ corresponding to the times $\{\tau_u, \tau_v, \tau_w\}$ taken for each LVLH component of position to reach and remain within some distance δ_{set}

*The components can, however, be succesfully decoupled by utilizing a PDD$^\alpha$ controller, containing both integer- and fractional-order derivatives.

	u	v	w	u'	v'	w'
IC1	-0.001	0	0	0	0.002	0.002
IC2	-0.001	0.002	-0.001	0	0.002	0
IC3	0.001	-0.002	0.001	0	0.002	-0.002

Table 1. Initial conditions used in this analysis (in non-dimensional coordinates).

of the equilibrium $\{u, v, w\} = 0$. For the coupled in-plane motion, in-plane settling time is defined as $s = n\tau$, with $\tau = \max(\tau_u, \tau_v)$.

- **Overshoot (OS):** the dimensionless quantity $\sigma_u = 1 + c|u|^{\max}$ (similarly defined for v and w components) where $|u|^{\max}$ is the magnitude of the largest extremum of distance from the equilibrium (not including the initial position). The constant value c is chosen from initial conditions to rescale $|u|^{\max}$ to an $\mathcal{O}(1)$ quantity. For the coupled in-plane motion, the overshoot is defined as the average of the u- and v-component overshoot, $\sigma = (\sigma_u + \sigma_v)/2$.

- **Integrated Control:** the dimensionless quantity found by integrating each component of the control effort,

$$U_u = \int_0^\infty |\upsilon_u(s)| ds \tag{24}$$

(similarly defined for v and w components). Note that this is representative of the total fuel cost used by the controller for the maneuver. For in-plane motion we will take the integrated control effort to be the sum $U = U_u + U_v$.

In the above definition of OS, unity is added to the extremal value to account for "overdamped" cases where the trajectory never overshoots the equilibrium; this is useful when computing combined performance measures using the geometric mean, as discussed below. Moreover, since this definition will be used for *comparison* of different trajectories, the specific scale c is largely inconsequential to the optimization results; nevertheless, for the initial conditions considered herein we universally set $c = 10^4$.

In what follows we will survey over the controller parameter space (comprising the controller gains and the fractional orders $\boldsymbol{\alpha}$) and compute the resulting controlled trajectory at each survey point. For each trajectory, some performance measure ψ will be computed; ψ will either be taken to be one of the above defined quantities (ST, OS, U), or some combination of two or more of these quantities. In the latter case we will compute the simultaneous performance measure as the geometric mean of the quantities; for instance, to characterize both ST and OS simultaneously, we will take $\psi = \sqrt{\text{ST} \times \text{OS}}$. Utilizing the geometric mean avoids complications that arise from differences in scale between ST, OS, and U. If, for instance, algebraic mean were instead used to define this combined performance measure, then the contributions from ST, OS, and U would be weighted differently; for example, since $U/\text{ST} \sim 10^{-3}$ for most trajectories considered herein, the algebraic mean would be much less sensitive to control effort.

As the in-plane and out-of-plane dynamics are uncoupled, these dynamics will be considered separately.

Out-of-plane motion

For the out-of-plane relative orbit motion, the controlled closed-loop dynamics are given by Eq. (19), repeated here for convenience:

$$w'' + k_{D_w} D^{\alpha_w} w + (1 + k_{P_w}) w = 0. \tag{19}$$

The controlled relative orbit trajectories obeying this equation can be computed using the FCC method provided initial conditions w_0 and w_0', which for the trajectories considered in this section are given in Table 1. The three tunable controller parameters are $\{\alpha_w,\ k_{P_w},\ k_{D_w}\}$, with $\alpha_w \in [0, 1]$, and the standard integer-order controller is recovered when $\alpha_w \to 1$.

As an initial demonstration, we first compute ST for the trajectory corresponding to IC1 while surveying over $\{\alpha_w, k_{P_w}, k_{D_w}\}$. We will survey over gains $\{k_{P_w}, k_{D_w}\} \in [0, 2]$, and within each α_w "slice" of control parameter space (with the $\alpha_w = 1$ slice corresponding to standard HCW PD control) we find the gain values which give rise to the smallest settling time. Note that qualitatively similar results were obtained if we extended the survey region to larger gains. In this scenario we will define settling time to be the time until the trajectory remains within $\delta_{\text{set}} = 10^{-5}$, which in physical units corresponds to a distance of 100 meters. Results of this survey, in the case of IC1, are shown in Fig. 2 as contour plots of settling time as a function of k_{P_w} and k_{D_w}. The left panel in this figure shows survey results for the standard integer-order controller, while the right panel of this figure shows the optimal slice of α_w parameter space ($\alpha_w = 0.91$). By direct comparison of the colored contours between the left and right panels, it can be seen that the right-hand panel corresponding to the fractional controller contains a region (upper-center of the panel) where ST is smaller than any point in the left-hand panel corresponding to standard control. In both slices we indicate the optimal settling time within that slice as a green star.

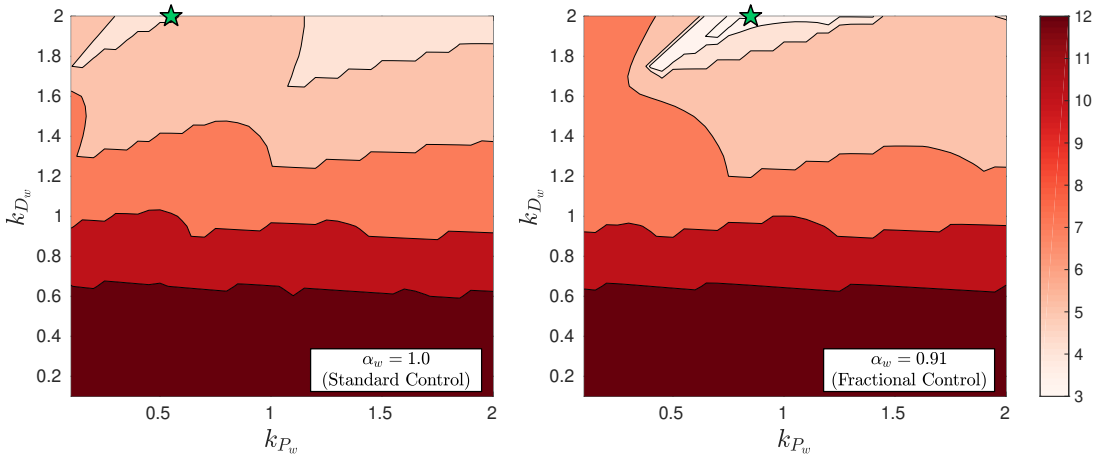

Figure 2. Settling time for IC1 as a function of controller gains k_{P_w} and k_{D_w}, at two different points in α_w-space. Optimal choices of gains are marked with a green star. At left we show the slice corresponding to standard PD control ($\alpha_w = 1$), while at right we show the optimal slice of α_w parameter space ($\alpha_w = 0.91$) corresponding to the fractional PD$^\alpha$ controller.

At these optimal choices of gains, we find a settling time of $\tau_w^{\text{int}} = 0.63 T_{\text{orb}}$ using the integer-order controller (at the optimal gains of $[k_{P_w}, k_{D_w}] = [0.55,\ 2.0]$), while for the slice corresponding to fractional control we find a settling time of $\tau_w^{\text{frac}} = 0.48 T_{\text{orb}}$ (at the optimal gains of $[k_{P_w}, k_{D_w}] =$

$[0.85,\ 2.0]$). This translates to a $\approx 24\%$ increase in performance. The trajectories for these two optimal cases are shown in the left panel of Fig. 3. We also show in this figure the settling time thresholds $w_{\rm set} = \pm 10^{-5}$ (dotted lines), along with the points along each trajectory corresponding to these settling times. It is clear from the figure that this performance improvement is not negligible, and the decrease in settling time does not come at the expense of noticeable increase in overshoot.

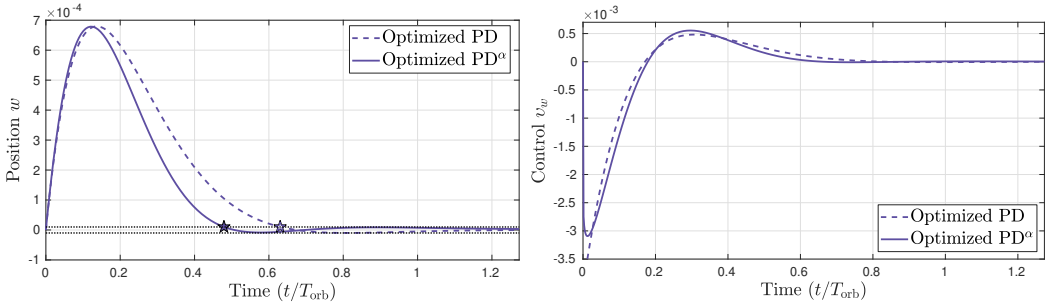

Figure 3. Trajectories which optimize settling time for both integer- and fractional-order control (left) along with corresponding control signals (right). Standard control is shown as the dotted lines, while fractional control is shown as solid lines. For reference, in the left panel we show the settling time threshold window as the black dotted lines and the points where the trajectories reach and remain within these windows as stars.

Moreover, it can be seen from the right panel of Fig. 3 that the decrease in settling time does not correspond to a substantial increase in control signal. We specifically find $U_w^{\rm int} = 0.00256$ and $U_w^{\rm frac} = 0.00264$, so that the fractional controller achieves a 24% faster settling time while only increasing integrated control by 3%.

Similar results are obtained from trajectories corresponding to IC2; for brevity, these contour and trajectory plots are not shown. In this case, we find the optimal ST using the standard controller is $\tau_w^{\rm int} = 0.56 T_{\rm orb}$ (at $[k_{P_w}, k_{D_w}] = [0.45,\ 2.0]$) and optimal ST using fractional controller is $\tau_w^{\rm frac} = 0.44 T_{\rm orb}$ (at $\alpha_w = 0.97$ and $[k_{P_w}, k_{D_w}] = [0.75,\ 1.95]$). Integrated control for these two cases is $U_w^{\rm int} = 0.00148$ and $U_w^{\rm frac} = 0.00147$. Thus in the case of IC2, we achieve a 22% reduction of settling time with a *simultaneous reduction* in integrated control. In the case of IC3, we find that ST is actually optimized using the standard controller, though as will be shown below this comes at the expense of an increase in U and/or OS.

A similar survey is now performed in order to simultaneously optimize ST, OS, and U. Thus in this case, the performance measure computed at each point in the survey is the geometric mean $\psi = ({\rm ST} \times {\rm OS} \times U)^{1/3}$. To illustrate how fractional control can achieve more optimal trajectories, we show in Fig. 4 the optimized ψ as a function of fractional order α_w for all three benchmark initial conditions listed in Table 1. The points along the right-hand side of this plot correspond to the standard controller ($\alpha_w = 1$). For all three benchmark ICs, we find that tuning α_w away from unity gives rise to more optimal trajectories in terms of the performance measure ψ.

The resulting optimized trajectories corresponding to Fig. 4, in the case of IC1 and IC2, are shown in Fig. 5. In the case of IC1, the numerical values of ST, OS, and U are separately tabulated below for both the optimized standard controller and optimized fractional controller ($\alpha_w = 0.91$):

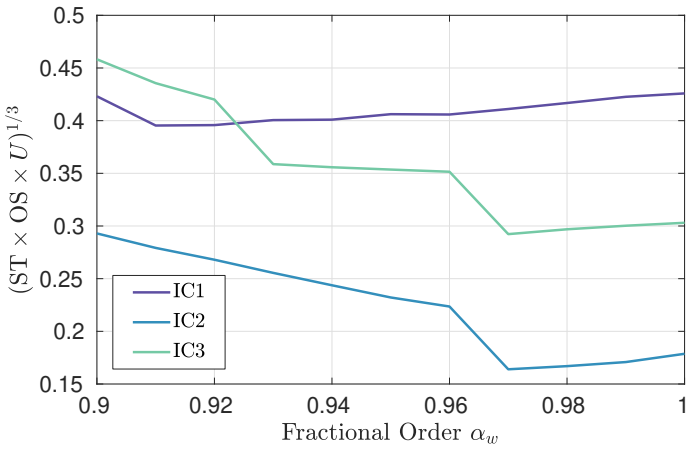

Figure 4. Combined performance measures for gain-optimized trajectories as a function of α_w. In all cases, tuning α_w away from unity reduces the geometric mean of settling time, overshoot, and integrated control.

IC1:	ST	OS	$U(\times 10^{-3})$
Optimized PD	4.12	6.87	2.726
Optimized PD$^{\alpha}$	3.01	7.78	2.637

In this case, utilizing fractional control gives rise to a $\approx$27% reduction in settling time while also reducing integrated control (fuel cost) by $\approx 3\%$. As illustrated both in the figure and in the table above, however, this comes at the expense of a 13% increase in OS.

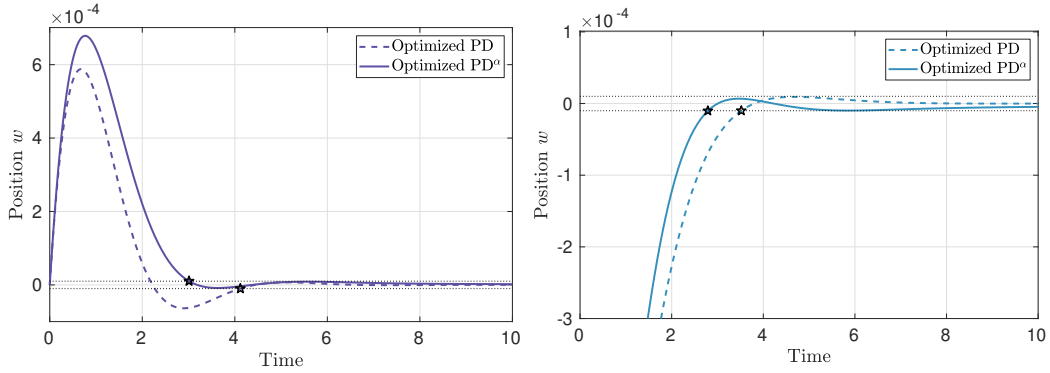

Figure 5. Optimized trajectories under both standard PD control (dashed lines) and fractional control for optimal α_w (solid lines). The left panel corresponds to IC1 and the right panel corresponds to IC2.

In the case of IC2, the numerical values of ST, OS, and U are again separately tabulated for both the optimized standard controller and optimized fractional controller ($\alpha_w = 0.97$):

IC2:	ST	OS	$U(\times 10^{-3})$
Optimized PD	3.52	1.093	1.483
Optimized PD$^{\alpha}$	2.79	1.067	1.480

In this case, utilizing fractional control gives rise to *simultaneous reduction* of ST ($\approx 21\%$), OS ($\approx 2.4\%$), and U ($\approx 0.2\%$).

In-plane motion

For the in-plane relative orbit motion, the controlled closed-loop dynamics are given by Eq. (16), again repeated here for convenience:

$$\boldsymbol{\zeta}' = \begin{bmatrix} \mathbf{0} & I_2 \\ \bar{A}_1 - \mathcal{K}_P & \bar{A}_2 \end{bmatrix} \boldsymbol{\zeta} - \begin{bmatrix} \mathbf{0} \\ \mathcal{K}_D \end{bmatrix} \begin{bmatrix} D^{\alpha_u} u \\ D^{\alpha_v} v \end{bmatrix}. \tag{16}$$

This controller now depends on 10 tunable parameters: the 8 gains within $\mathcal{K}_P$ and $\mathcal{K}_D$, along with the two fractional orders of the u- and v-components, α_u and α_v. Due to the large dimension of the controller parameter space, it is clear that a similar grid-based survey as used above will in this case not be feasible: if we desire p grid-points per tunable parameter, the amount of grid-points in such a survey is 10^p. This so-called "curse of dimensionality" prevents survey resolutions of any reasonable resolution. Thus in this case a more structured optimization algorithm is needed in order to optimize a given performance measure ψ.

This is in fact an example of a non-convex optimization problem, since for a given optimization goal there typically exists many local optima within the 8-dimensional gain parameter space. As the goal of this work is simply to provide *proof-of-principle* examples showing that fractional control can outperform standard control, we have chosen to use a simple pattern-search algorithm to find, for a given ψ, the closest *local* optimum to some benchmark point in parameter space. Specifically, we choose some initial *seed* gain matrix $\mathcal{K}^{(0)} = [\mathcal{K}_P^{(0)}\ \mathcal{K}_D^{(0)}]$ corresponding to a well-behaved region of gain space, and use this seed matrix recursively to explore the parameter space about this point in gain space and as $\{\alpha_u, \alpha_v\}$ is tuned away from unity. Optimal controllers in terms of some performance measure ψ will then be found within this region.

The specific pattern search algorithm we have used is described as follows:

1. Denote the elements of a given gain matrix as k_m, $m = 1, 2, \ldots, 8$. Starting from a seed matrix $\mathcal{K}^{(i)}$ with elements $k_m^{(i)}$, integrate the 2D HCW trajectory and compute the desired performance measure $\psi^{(i)}$.
2. From $\mathcal{K}^{(i)}$ define the 16 test gain matrices $\mathcal{K}_{m\pm}^{\text{test}}$ by adjusting each element separately, $k_m^{\text{test}} = k_m^{(i)} \pm \delta k$, for $m = 1, 2, \ldots, 8$. Compute the 16 performance measures $\psi_{m\pm}^{\text{test}}$ associated with $\mathcal{K}_{m\pm}^{\text{test}}$.
3. Find $\psi^* = \min(\psi^{(i)}, \{\psi_{m\pm}^{\text{test}}\})$. If $\psi^* = \psi^{(i)}$, the algorithm terminates and $\mathcal{K}_{\text{opt}} = \mathcal{K}^{(i)}$. Otherwise, set $\mathcal{K}^{(i+1)} = \mathcal{K}^*$, where $\mathcal{K}^*$ is the gain matrix corresponding to ψ^*.
4. If the algorithm has not terminated at step 3, relabel $i + 1 \to i$ and return to step 2.

A convenient seed matrix is that corresponding to the LQR optimal gain matrix corresponding to the cost functional Eq. (23), choosing the state and control matrices (Q and R, respectively) to be identity matrices; these choices will, roughly speaking, lead to well-balanced trajectories with low values of settling time, overshoot, and integrated control. For these choices of Q and R, the LQR-optimized HCW gain matrix is explicitly given by

$$\mathcal{K}_{LQR} = \begin{bmatrix} 4.00 & -0.95 & 2.40 & 0.65 \\ 3.00 & 0.30 & 0.65 & 1.95 \end{bmatrix}.$$

This choice for our seed matrix is especially convenient since it is independent of initial conditions. To find the optimized gain matrix for standard PD control, $\mathcal{K}_{\rm opt}(\alpha_u, \alpha_v) = \mathcal{K}_{\rm opt}(1.0, 1.0)$, an initial run of the above algorithm with $\delta k = 0.1$ is then followed by a refined run using $\delta k = 0.05$. We have confirmed that the above algorithm is largely insensitive to the choice of the initial ("rough") grid resolution. Additionally, to prevent "run-away" scenarios where the algorithm simply increases specific gains without bound, we have also restricted our search region to gains $k_m \in [-8, 8]$, $m = 1, 2, \ldots, 8$.

The optimal gain matrices $\mathcal{K}_{\rm opt}(\alpha_u, \alpha_v)$ for the fractional controller are found using the same algorithm. Since the resulting trajectory is in fact highly sensitive to small changes in both gain matrix $\mathcal{K}$ and fractional orders $\{\alpha_u, \alpha_v\}$, we first sample points in the parameter space neighboring the standard PD controller (*i.e.*, $(\alpha_u, \alpha_v) = \{(1.0, 0.99),\ (0.99, 1.0), \ldots\}$) and use $\mathcal{K}_{\rm opt}(1.0, 1.0)$ as the algorithm seed matrix; one pass of the algorithm with $\delta k = 0.05$ is used. These optimized gain matrices in turn are then used as seed matrices for neighboring points in $\{\alpha_u, \alpha_v\}$-space farther away from unity.

We will first consider trajectories generated from IC1, and simultaneously optimize both ST and OS. That is, we find for each choice of $\{\alpha_u, \alpha_v\}$ the gain matrix that minimizes $\psi = \sqrt{\rm ST \times OS}$. For standard PD control, this gain matrix is found through the above pattern-search algorithm as

$$\mathcal{K}_{\rm opt}(\alpha_u, \alpha_v) = \mathcal{K}_{\rm opt}(1, 1) = \begin{bmatrix} 4.00 & -1.35 & 2.40 & 0.65 \\ 3.15 & 0.40 & 0.70 & 1.95 \end{bmatrix},$$

which provides $\sqrt{\rm ST \times OS} = 3.5517$. A survey is performed over all values of $\{\alpha_u, \alpha_v\} \in [0.90, 1.00]$ (with a survey resolution of $\delta\alpha = 0.01$) in order to determine if this performance measure can be further reduced by utilizing fractional control. Results of this survey are shown as a contour plot in the left panel of Fig. 6; each point on this plot shows the optimal geometric mean of ST and OS for the corresponsing choice of $\{\alpha_u, \alpha_v\}$. (Note that these contour plots utilize a blue color scheme to differentiate them from Fig. 2, the latter of which shows contour lines in 2D gain space.) We find that this geometric mean is optimized for $\{\alpha_u, \alpha_v\} = \{0.99, 0.90\}$, giving $\sqrt{\rm ST \times OS} = 3.1847$; this corresponds to a $\approx 23\%$ reduction in the performance measure. The gain matrix corresponding to this point, as found by the pattern search algorithm, is given by

$$\mathcal{K}_{\rm opt}(\alpha_u, \alpha_v) = K_{\rm opt}(0.98, 0.90) = \begin{bmatrix} 4.10 & -1.55 & 2.70 & 1.05 \\ 3.15 & 0.90 & 0.90 & 2.05 \end{bmatrix}.$$

In this case, both ST and OS are *separately* reduced by using fractional control: we find a reduction in ST of 26% and a reduction in OS by 20%

The same analysis is performed for trajectories corresponding to IC2 and IC3; optimal gain matrices for these cases are omitted for brevity. For IC2 we find a 17% reduction in the performance measure by using a fractional controller with $\{\alpha_u, \alpha_v\} = \{0.96, 0.93\}$, with ST reduced by 5% and OS reduced by 28%. For IC3 we find an 12% reduction in $\sqrt{\rm ST \times OS}$ by using a fractional controller with $\{\alpha_u, \alpha_v\} = \{0.97, 0.90\}$, with ST reduced by 24%; in this case, however, OS is slightly increased (by 1%). The results of this latter survey are shown in the right panel of Fig. 6. Note that in both cases (IC1 and IC3), it is apparent from Fig. 6 that reducing the fractional orders α_v below 0.90 can potentially reduce the performance measure even further.

The optimized trajectories corresponding to the green stars in Fig. 6 are explicitly shown in Fig. 7. The settling time threshold is again shown as black dotted lines. In both cases it can be seen that both

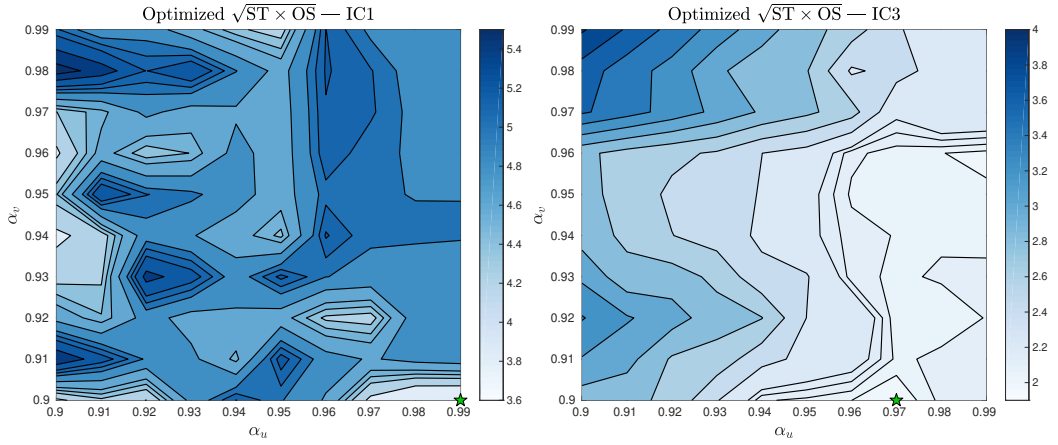

Figure 6. Contour plots showing the optimized geometric mean of ST and OS, as a function of fractional control orders α_u and α_v. The left panel corresponds to IC1 while the right panel corresponds to IC3.

settling time (as marked by the correspondingly-colored stars) and overshoot are simultaneously reduced by utilizing fractional control. Note that since settling time for in-plane motion is defined as the larger of the settling times in the u and v dimensions, only one star per trajectory is shown.

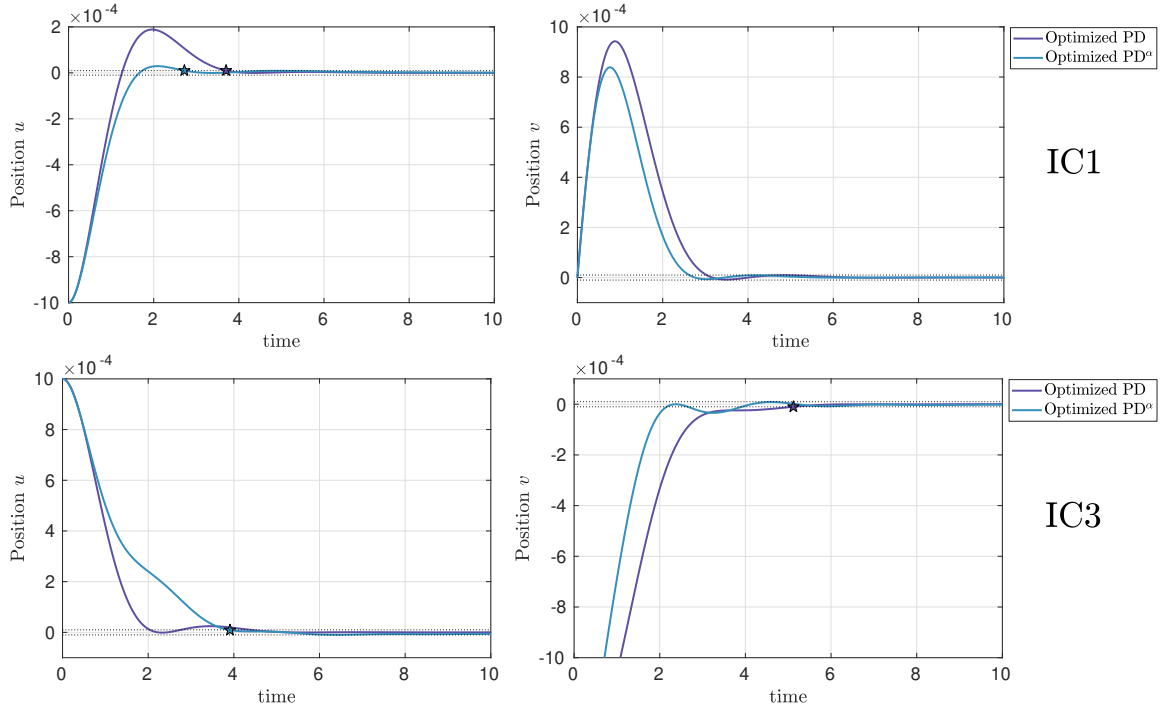

Figure 7. $\sqrt{\mathrm{ST} \times \mathrm{OS}}$-optimized trajectory components for standard PD control (purple) and fractional PD$^\alpha$ control (blue). Top panels show trajectory components corresponding to IC1 and bottom panels show components corresponding to IC3. The points on the trajectories which define settling time are marked with stars.

Although the above survey demonstrates that both ST and OS can be reduced by introducing fractional control, in many of these cases this reduction comes at the expense of an increase in

integrated control effort. Therefore, to demonstrate that more optimal trajectories can be achieved *without* a corresponding increase in integrated control, we have performed a second survey which optimizes $\sqrt{\mathrm{ST} \times \mathrm{U}}$. The optimal gain matrices for both standard and fractional control differ in general from those found in the previous optimization survey, and are again omitted for brevity. The results of this survey are shown as contour plots in Fig. 8.

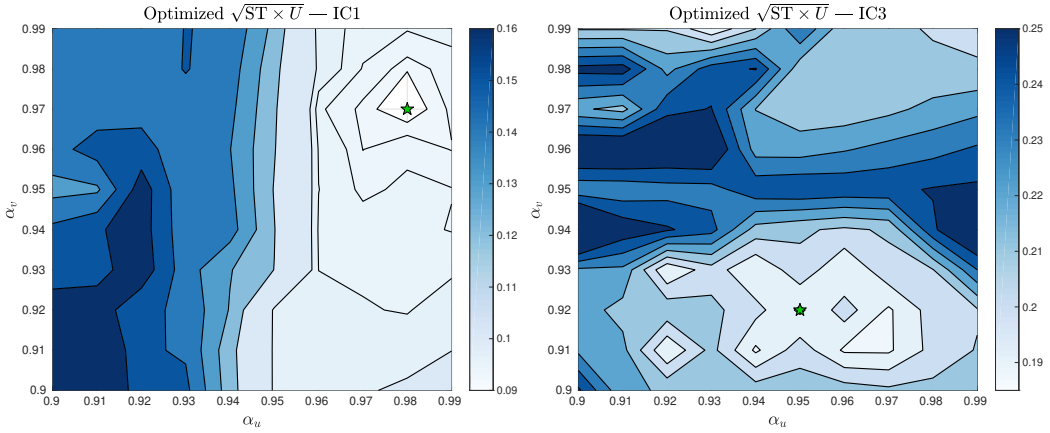

Figure 8. Contour plots showing the optimized geometric mean of ST and U, as a function of fractional control orders α_u and α_v. The left panel corresponds to IC1 while the right panel corresponds to IC3.

For IC1, the performance measure $\sqrt{\mathrm{ST} \times U}$ corresponding to the optimized standard and fractional controllers is 0.0949 and 0.0925, respectively, giving a reduction of 2.5%. Although the geometric mean is reduced, settling time is actually increased (3.79 to 4.00) while integrated control is decreased (0.0024 to 0.0021).

For IC3, optimized $\sqrt{\mathrm{ST} \times U}$ for standard and fractional controllers is 0.2013 and 0.1880, respectively, corresponding to a 6.5% reduction by utilizing fractional control. In this case, settling time is substantially reduced from 4.03 to 3.28, while integrated control effort is only marginally increased from 0.0101 to 0.0108. The components of this trajectory are shown in Fig. 9. Incidentally, in this case overshoot is also substantially reduced.

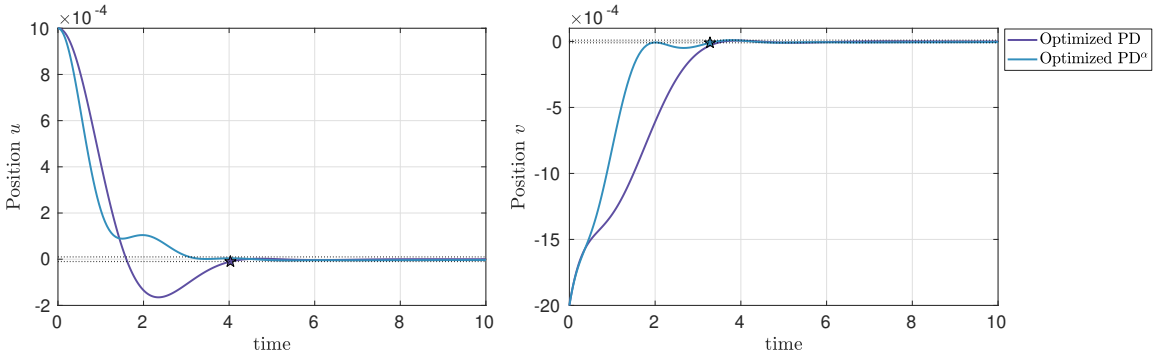

Figure 9. Optimized trajectory components for standard PD control (purple) and fractional PD$^\alpha$ control (blue) for IC3. The fractionally controlled trajectory reduces settling time by 18% while increasing integrated control by only 7%.

The above results demonstrate the additional freedom in trajectory shaping that one is afforded by

utilizing fractional PD$^\alpha$ controllers in place of standard PD controllers for relative-orbit dynamics. These proof-of-principle examples establish that this freedom allows one to design trajectories and control histories which are more optimal with respect to various performance measures.

CONCLUSION

In this work we explored the generalization of standard PD-type controllers for HCW relative-orbit dynamics by introducing fractional derivatives into the feedback control laws. As demonstrated herein, the orders $\{\alpha_u, \alpha_v, \alpha_w\}$ of these fractional derivative terms serves as additional tunable parameters, allowing more freedom in how one can shape the controlled trajectory of the deputy in its relative orbit. This additional freedom can be used to achieve faster and more direct rendezvous maneuvers as compared to standard integer-order controllers, while simultaneously using less fuel.

These benefits were illustrated for three benchmark scenarios corresponding to three different sets of relative-orbit initial conditions. By simultaneously optimizing settling time, overshoot, and integrated control effort, it was shown that fractional control for out-of-plane motion achieved more optimal trajectories in all three benchmark cases. Among these results, the optimal fractional controller separately reduced ST, OS, and U with respect to integer-order control by 21%, 2.4%, and 0.2% respectively. Similar results were shown for the coupled in-plane motion, where the use of fractional controllers substantially reduced the various performance measures with only marginal increase in fuel cost.

Although in this work only circular chief orbit configurations were considered, there is nothing preventing the utilization of these fractional PD$^\alpha$ controllers in cases where the chief orbit is elliptical. In this case, however, the control law Eq. (15) must be added component-wise to the Tschauner-Hemple (TH) equations[1] (which reduce to the HCW equations when eccentricity $e \to 0$); the resulting trajectories can still be integrated using the FCC method as done in this work. In this case, however, the proof of stability discussed in this work fails as the system is no longer time-invariant. One interesting approach to this problem is to transform the TH dynamics to an equivalent system obeying HCW dynamics through the use of Lyapunov-Floquet transformations.[26] Applying this approach for fractionally-controlled relative-orbit trajectories is left as a topic for future work.

Regardless of the simplifying assumptions and specific control design strategy we have used, the benchmark examples we have considered demonstrate as a proof-of-principle that fractional PD$^\alpha$ controllers can outperform standard PD controllers for the maneuvering of relative-orbit trajectories.

ACKNOWLEDGMENT

We thank Ethan Burnett for useful discussions. E.B. and D.Y. are grateful for the hospitality of the Air Force Research Lab at Kirtland AFB during the 2018 Summer Faculty Fellowship Program.

REFERENCES

[1] K. T. Alfriend, S. R. Vadali, P. Gurfil, J. P. How, and L. S. Breger, *Spacecraft Formation Flying*. Oxford, UK: Elsevier Ltd., 2010.

[2] H. Schaub and J. Junkins, *Analytical Mechanics of Space Systems*. Reston, VA: American Institute of Aeronautics and Astronautics, Inc., 2009.

[3] K. B. Oldham and J. Spanier, *The Fractional Calculus*. San Diego, Californa: Academic Press, Inc., 1974.

[4] K. S. Miller and B. Ross, *An Introduction to the Fractional Calculus and Fractional Differential Equations*. New York, New York: John Wiley & Sons, Inc., 1993.

[5] N. Wheeler, "Construction and Physical Application of the Fractional Calculus," February 1997. Reed College lecture notes.

[6] Y. Chen, I. Petras, and D. Xue, "Fractional Order Control – A Tutorial," *2009 American Control Conference*, 2009, pp. 1397–1411, 10.1109/ACC.2009.5160719.

[7] R. E. Gutierrez, J. M. Rosario, and J. T. Machado, "Fractional Order Calculus: Basic Concepts and Engineering Applications," *Mathematical Problems in Engineering*, Vol. 3758, 2010, 10.1155/2010/375858.

[8] R. L. Bagley and R. A. Calico, "Fractional Order State Equations for the Control of Viscoelastically Damped Structures," *Journal of Guidance, Control, and Dynamics*, Vol. 14, No. 2, 1991, pp. 304–311.

[9] A. Oustaloup, *La commande CRONE: Commande Robuste d'Ordre Non Entier*. Paris: Herme's, 1991.

[10] I. Podlubny, "Fractional-order systems and $PI^{\lambda}D^{\mu}$-controllers," *IEEE Transactions on Automatic Control*, Vol. 44, No. 1, 1999, pp. 208–214, 10.1109/9.739144.

[11] D. Matignon, "Stability Results for Fractional Differential Equations with Applications to Control Processing," *Computational Engineering in Systems Applications*, July 1996, pp. 963–968.

[12] D. Yaylali, E. A. Butcher, and A. Dabiri, *Fractional PID Consensus Control Protocols for Second-Order Multiagent Systems*. San Diego, CA: AIAA Guidance, Navigation, and Control Conference, 2019. Accepted for inclusion, June 2018.

[13] D. Xue, C. Zhao, and Y. Chen, *Fractional order PID control of a DC-motor with elastic shaft: a case study*. Minneapolis, MN: Proceedings of the American Control Conference, 2006, 10.1109/ACC.2006.1657207.

[14] E. A. Butcher, M. Nazari, A. Dabiri, and A. K. Sanyal, *Fractional PID Control of Spacecraft Attitude Dynamics using Rotation Matrices*. IAC, Guadalajara: Proceedings of the International Astronautical Congress, 2016.

[15] M. Nazari, E. A. Butcher, and A. K. Sanyal, "Spacecraft Attitude Fractional Feedback Control using Rotation Matrices and Exponential Coordinates," *Journal of Guidance, Control, and Dynamics*, Vol. 41, 2018, pp. 2185–2198.

[16] M. Nazari, E. A. Butcher, and A. K. Sanyal, *Fractional Control of Rigid Body Attitude Dynamics using Exponential Coordinates*. Kissimmee, FL: AIAA Guidance, Navigation, and Control Conference, 2018.

[17] W. H. Clohessy and R. S. Wiltshire, "Terminal Guidance System for Satellite Rendezvous," *Journal of the Aerospace Sciences*, Vol. 27, No. 9, 1960, pp. 653–658.

[18] A. J. Sinclair, R. E. Sherrill, and T. A. Lovell, "Calibration of Linearized Solutions for Satellite Relative Motion," *Journal of Guidance, Control, and Dynamics*, Vol. 37, No. 4, 2014, pp. 1362–1367.

[19] A. J. Sinclair, R. E. Sherrill, and T. A. Lovell, "Use of Cartesian-Coordinate Calibration for Satellite Relative-Motion Control," *Journal of Guidance, Control, and Dynamics*, Vol. 38, No. 9, 2015, pp. 1842–1847.

[20] I. Podlubny, *Fractional Differential Equations*. San Diego: Academic Press, 1999.

[21] A. Dabiri and E. A. Butcher, "Efficient Modified Chebyshev differentiation Matrices for Fractional Differential Equations," *Communications in Nonlinear Science and Numerical Simulation*, Vol. 50, 2017, pp. 584–610.

[22] A. Dabiri and E. A. Butcher, "Stable Fractional Chebyshev Differentiation Matrix for Numerical Solution of Fractional Differential Equations," *Nonlinear Dynamics*, Vol. 90, No. 1, 2017, pp. 185–201.

[23] D. Valerio and J. S. d. Costa, *An Introduction to Fractional Control*. London: The Institution of Engineering and Technology, 2013, 10.1049/PBCE091E.

[24] O. P. Agrawal, "A general formulation and solution scheme for fractional optimal control problems," *Nonlinear Dynamics*, Vol. 38, No. 1-4, 2004, pp. 323–337.

[25] S. Pooseh, R. Almeida, and D. F. M. Torres, "Fractional Order Optimal Control Problems with Free Terminal Time," *ArXiv e-prints*, Feb. 2013.

[26] R. E. Sherrill, A. J. Sinclair, S. Sinha, and T. A. Lovell, "Lyapunov-Floquet Control of Satellite Relative Motion in Elliptic Orbits," *IEEE Transactions on Aerospace and Electronic Systems*, Vol. 51, No. 4, 2015, pp. 2800–2810.